http://dx.doi.org/10.5012/bkcs.2013.34.11.3269

Graphene Oxide as a Novel Nanoplatform for Direct Hybridization of Graphene-SnO_2

Hun Park and Tae Hee Han*

Department of Organic and Nano Engineering, Hanyang University, Seoul 133-791, Korea
**E-mail: than@hanyang.ac.kr*
Received June 19, 2013, Accepted August 12, 2013

Graphene oxide (GO) has been of particular interest because it provides unique properties due to its high surface area, chemical functionality and ease of mass production. GO is produced by chemical exfoliation of graphite and is decorated with oxygen-containing groups such as phenol hydroxyl, epoxide groups and ionizable carboxylic acid groups. Due to the presence of those functional groups, GO can be utilized as a novel platform for hybrid nanocomposites in chemical synthetic approaches. In this work, GO-SnO_2 nanocomposites have been prepared through the spontaneous formation of molecular hybrids. When SnO_2 precursor solution and GO suspension were simply mixed, Sn^{2+} was spontaneously formed into SnO_2 nanoparticles upon the deoxygenation of GO. Through further chemical reduction by adding hydrazine, reduced GO-SnO_2 hybrid was finally created. Our investigation for the electrocapacitive properties of hybrid electrode showed the enhanced performance (389 F/g), compared with rGO-only electrode (241 F/g). Our approach offers a scalable, robust synthetic route to prepare graphene-based nanocomposites for supercapacitor electrode *via* spontaneous hybridization.

Key Words : Graphene oxide, SnO_2, Supercapacitors, Hybrid, Nanocomposites

Introduction

Graphene oxide (GO) is commonly made by reacting graphite powders with strong oxidation agents and acids.[1,2] During this process, graphene is oxidized and derivatized with oxygen containing functional groups, and consequently is readily exfoliated from graphite into single GO layer in water.[3,4] However, the presence of functional groups including hydroxyl, epoxide, and carboxylic acid groups on a carbon sheet and amorphous carbon regions on basal plane causes this carbon sheet to be electronically insulating. Therefore, considerable works have been focused on recovering the poor electrical properties of GO through the development of efficient reducing strategies or the exclusion of harsh oxidation steps for realizing the highly motivated properties of pristine graphite.[5-7] Despite those disadvantageous properties, however, GO has attracted increasing research interest owing to its unique properties including large surface area, high water solubility, facile processibility, and easy large-scale production.[8-11] In particular, the functional groups of GO may play an important role in facilitating molecular organization into functional hybrid nanocomposites.[12]

A variety of metal oxides, such as MnO_x, RuO_x, and CuO_x, with pseudo-capacitive properties have been used to form nanocomposites with graphene and have been utilized in supercapacitors because of the improved capability to store more charges than carbon-only electrodes.[13-16] Up to date, the preparation methods including hydrothermal synthesis or a polyol process have been successfully achieved to create nanocomposites.[17-20] However, the development of a scalable, robust synthetic process is still required to achieve the practical utilization of graphene into high performance supercapacitors.

In this work, we introduce a straightforward preparation approach to prepare a hybrid of graphene and SnO_2 *via* the directed hybridization. SnO_2 has attracted much attention as an excellent electrode material for supercapacitors and secondary Li-ion batteries due to its interesting properties of high theoretical capacity, good electroconductivity and low cost.[21,22] GO was first prepared through chemical exfoliation of graphite and was mixed with a SnO_2 precursor solution. During solution mixing, the reduction of GO and the conversion of SnO_2 nanoparticles from Sn^{2+} occur simultaneously. After further reduction of GO by adding hydrazine and thermal annealing, nanocomposites (rGO-SnO_2) were created. Hybrid materials showed the increased supercapacitance values and the more stable electrochemical performance over a wide range of voltage scan rates, compared with the rGO-only electrode.

Experimental

Materials. Graphite powders were purchased from Bay carbon (SP-1). Other chemicals, including hydrazine, hydrochloride, sulfuric acid, hydro peroxide, and tin acetate ($Sn(CH_3COO)_2$), were purchased from Sigma-Aldrich. All chemicals were used as received without additional purification.

Synthesis of GO. GO was prepared using a modified Hummers method from graphite powder as reported elsewhere.[10-12] An aqueous GO dispersion was extensively washed and filtered with 1 M HCl and then was dialyzed with a dialysis membrane (Spectra Dialysis Membrane, MWCO: 6-

8,000) to remove the salt byproduct and excess acid. After dialysis, the viscous GO solution was diluted in deionized water (DI) and was put in a water-bath-sonicator for monolayer exfoliation. The concentration of the resulting GO solution was 3.2 mg/mL.

Synthesis of Graphene-SnO_2 Nanocomposites. Tin acetate ($Sn(CH_3COO)_2$) was dissolved in a 1:10 DI/MeOH mixture at 20 mg/mL. Then, 3 mL of the SnO_2 precursor solution was added dropwise into 40 mL of the GO solution (3.2 mg/mL) under vigorous stirring at room temperature. To measure sheet resistivity of hybrid, the nanocomposites film of 10 μm thickness was prepared with a vacuum filtration kit using a hydrophilic PTFE membrane (Millipore, pore size: 450 nm). For further reduction of composites, 30 μL of hydrazine (Sigma-Aldrich, 64%) was added into a GO-SnO_2 solution and mechanically stirred at 70 °C for 2 h. The finally obtained rGO-SnO_2 nanocomposites were annealed at 400 °C for 2 h under air.

Characterization. The morphologies of the nanocomposites were characterized with a scanning electron microscopy (JEOL JSM-6701F) and a transmission electron microscopy (JEOL JEM-2100F). TEM samples were prepared by dispersing a small amount of the nanocomposite powder in MeOH with sonication and then applying a few drops of the dispersion onto a lacey-carbon TEM grid (Ted Pella, Inc.). Thermogravimetric analysis (TGA) was performed on SDT Q600 (TA Instruments) in the temperature range between 25 and 800 °C at a heating rate of 10 °C/min under air atmosphere. X-ray diffraction (XRD) was carried out using Cu Kα radiation (λ = 1.5418 Å). X-ray photoelectron spectroscopy (XPS) measurements were carried out using a Thermo Scientific Theta probe with monochromatic Al Kα radiation. Sheet resistivity of hybrid films was measured with Advanced Instrument Technology (CMT-Series).

Electrochemical Measurements. The electrochemical behavior of rGO and rGO-SnO_2 was characterized by cyclic voltammetry (CV) and galvanostatic charge-discharge measurements using a Bio-Logic (SP-200) in 1 M H_2SO_4 electrolyte. The working electrode was prepared by dropping 10 μL of active material solution (5.0 mg/mL) in NMP onto the glassy carbon electrodes. Prior to experiments, the electrolyte was purged with pure N_2 gas for 30 min to remove dissolved oxygen. Experiments were carried out in a three-electrode glass cell at room temperature. Platinum foil was used as a counter electrode and an Ag/AgCl electrode as the reference electrode.

Results and Discussion

As shown in Figure 1(a), the GO solution was brown in color, and there was no precipitation. To prepare a GO-SnO_2 hybrid, a tin acetate ($Sn(CH_3COO)_2$) precursor solution was added dropwise under vigorous mechanical mixing. As soon as the tin acetate solution was added, the GO solution became viscous, as shown in images of Figure 1(b) and (c). When the concentration of GO was higher than 4.0 mg/mL or the precursor solution of 20 mg/mL was added more than

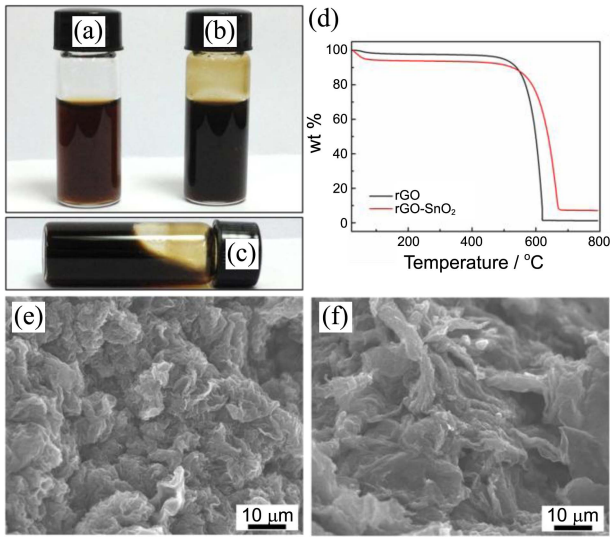

Figure 1. Hybrid assembly of GO-SnO_2 hybrid. a-c) Photographs of the sample: aqueous GO suspension (a) and GO-SnO_2 complex (b) after mixing. GO solution became viscous and dark brown color (c). By adding a small amount of hydrazine GO was reduced, and then thermally annealed to enhance the crystallinity of SnO_2. d) TGA curves of the reduced GO (rGO) and rGO-SnO_2. e and f) SEM images of rGO-SnO_2 nanocomposites before (e) and after thermal annealing (f).

3.0 mL, the complex easily formed a gel. This change in the fluidity of the mixture solution is due to the formation of the molecular networks between carbon sheets and SnO_2 nanoparticles, as often exhibited in the percolated solution of hydro-/organo-gels.[23-25] In this work, the concentration of GO and tin acetate solution was kept consistently under the gel-forming critical concentration to avoid heterogeneous mixing. In addition, the color of GO suspension changed to dark brown, which further indicates the deoxygenation of GO. Compared with insulating GO paper, thin films of GO-SnO_2 hybrid showed a much lower sheet resistivity of 8.2×10^6 Ω/sq. due to the reduction effect of GO and the presence of the electroconductive SnO_2 nanoparticles on GO sheet. The further reduction of GO was carried out by loading a small amount of hydrazine solution, and the reduced GO (rGO)-SnO_2 hybrid composites were annealed to enhance the crystallinity of SnO_2 nanoparticles at 400 °C. The weight ratio of SnO_2 nanoparticles in the hybrid was verified with TGA (Figure 1(d)). A significant weight loss between 400 and 700 °C is attributed to the decomposition of the carbon sheets.[26] Based on the TGA result, it is confirmed that the hybrid contains SnO_2 nanoparticles of approximately 6.8 wt %.

The morphology of the rGO-SnO_2 hybrid was characterized by field emission scanning electron microscopy (FE-SEM) before and after annealing, as shown in Figure 1(e) and (f), respectively. We note that, though the surface of hybrid composites is quite roughened and crumpled before annealing (Figure 1(e)), the rough surface wasn't entirely flattened and the nanocomposites didn't agglomerate even after high temperature annealing (Figure 1(f)).

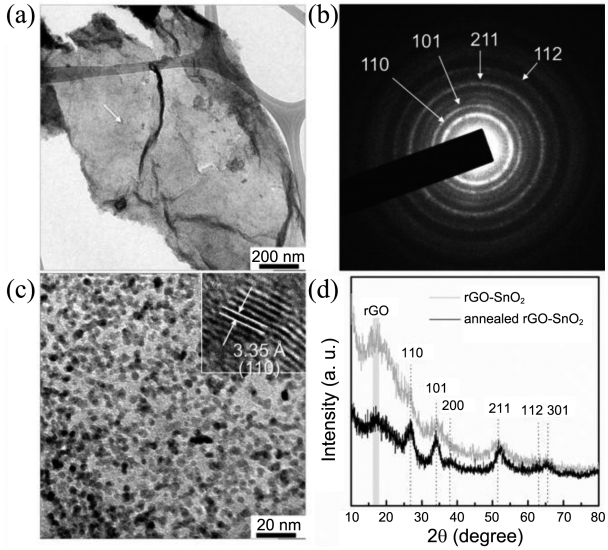

Figure 2. Crystalline morphology of the hybrid. (a) TEM image of isolated rGO-SnO_2 nanocomposites. (b) A selected area electron diffraction (SAED) pattern of hybrid (a). (c) A magnified HRTEM image corresponding to the pointed region with a white arrow in (a). The inset image of (c) shows the crystal lattice fringes of highly crystalline SnO_2 nanoparticles. The crystalline lattice spacing is 3.35 Å corresponding to the (110) lattice plane of a cassiterite SnO_2 crystal. (d) X-ray diffraction of rGO-SnO_2 nanocomposites. XRD pattern of hybrid has six well-resolved peaks assigned as the diffraction peaks of cassiterite of SnO_2 phase (JCPDS No. 41-1445). The peaks of the sample annealed at 400 °C for 2 h were greatly enhanced.

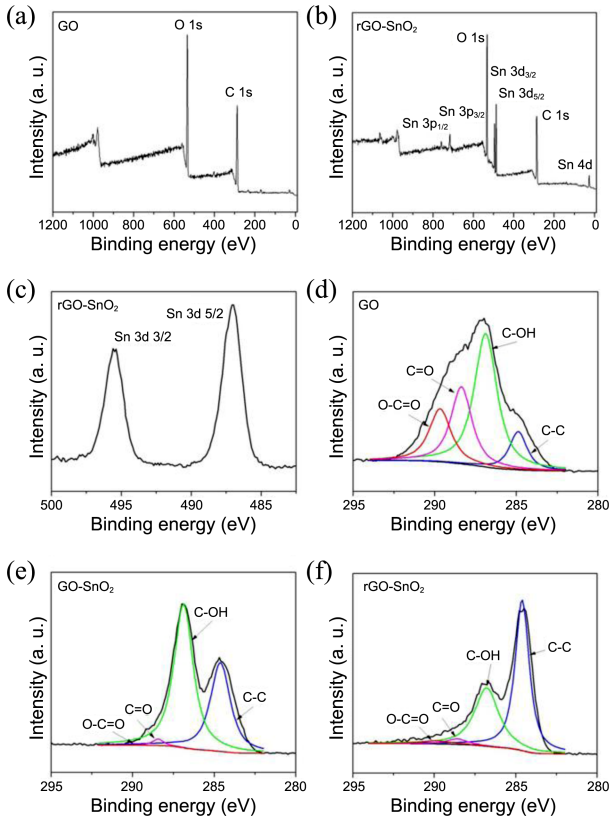

Figure 3. XPS patterns of the GO (a) and rGO-SnO_2 nanocomposites (b). c) The Sn 3d spectrum of the prepared rGO-SnO_2 nanocomposite. The C 1s XPS spectra of the GO (d), GO-SnO_2 nanocomposites (e), and rGO-SnO_2 nanocomposites (f).

The crystalline structure of the annealed SnO_2 nanoparticles and their spatial distribution over carbon sheets were examined with the high-resolution transmission electron microscopy (HR-TEM). Figure 2(a) shows the isolated single layer of rGO-SnO_2 hybrid. The rGO was uniformly coated with SnO_2 nanoparticles and this nanocomposite was not densely aggregated. As shown in the higher magnification image (Figure 2(c)) of the indicated region with a white arrow in Figure 2(a), the size of SnO_2 particles was 3-5 nm in diameter and evenly dispersed throughout the rGO sheet. It should be noted that the structure of well-distributed nanoparticles over rGO sheets improves electron transfer, resulting in enhanced electrochemical properties. Figure 2(b) shows the selected area electron diffraction (SAED) pattern of the rGO-SnO_2 hybrid; this result is consistent with a typical electron diffraction pattern for cassiterite SnO_2 (Figure 2(d)). As shown in Figure 2(c), the crystal lattice fringes were observed over the entire sample, demonstrating the high crystallinity of SnO_2 nanoparticles. As indicated in the inset image of Figure 2(c), the crystalline lattice spacing of 3.35 Å is distinct. This corresponds to the (110) lattice plane of a cassiterite SnO_2 crystal.

Figure 2(d) presents the powder X-ray diffraction (XRD) patterns of rGO-SnO_2 nanocomposites with six well-resolved diffraction peaks. Those peaks are typical diffraction peaks from the (110), (101), (200), (211), (112) and (301) crystalline lattice planes of the cassiterite of SnO_2 phase (JCPDS 41-1445, a = 4.7382 Å, c = 3.1871 Å). An average crystallite size of 3.3 nm was calculated using the Scherrer equation:

$$L = \frac{0.9\lambda}{B(2\theta)\cos(\theta)} \quad (1)$$

where L is the crystallite size and $B(2\theta)$ is the line width. The value is completely consistent with the results of TEM characterization. The intensity of the crystalline SnO_2 peaks increased after thermal annealing. The most intense peak of rGO (at around $2\theta = 16.9°$) indicates much larger interlayer spacing (0.41 nm), compared with the pristine graphite (0.34 nm).

Figure 3(a) and (b) show the full range XPS spectra of GO and rGO-SnO_2 hybrid, respectively. As presented in Figure 3(b), the Sn 3p, 3d, 4s, 4p, and 4d peaks appear due to the presence of SnO_2 nanoparticles, and the peak of C 1s is attributed to rGO.[27] In the high-resolution Sn 3d XPS spectrum in Figure 3(c), peaks of Sn $3d_{3/2}$ and Sn $3d_{5/2}$ are at 487.3 and 495.7 eV, with an 8.4 eV peak-to-peak separation, which indicates the formation of SnO_2 nanoparticles on graphene.[28] The C 1s XPS spectra of GO and hybrid nanocomposites are shown in Figure 3(d)-(f). The bands at 287-289 eV corresponding to the oxygenated functional groups were definitely shown in Figure 3(d).

Compared with GO, the C 1s XPS spectrum of the GO-SnO_2 nanocomposites (Figure 3(e)) shows a significant

increase in the intensity of C-C at 284.7 eV and the much smaller amount of oxygen-containing functionalities, indicating a successful deoxygenation. It implies that the GO plays a key role for hybridization as an oxygen-provider to form SnO_2 nanoparticles. In addition, as confirmed in Figure 2(a) and (c), the even distribution of SnO_2 on graphene sheet indicates the presence of abundant oxygen-containing defect sites throughout the basal plane and edges of GO.[11] Adding hydrazine in a GO-SnO_2 composite suspension resulted in suppressed oxygen-related peaks, indicating the further reduction of GO (Figure 3(f)). However, at the end of the reduction, these peaks did not completely disappear. This is due to the screening effect of SnO_2 nanoparticles attached to carbon sheets for an access of hydrazine to some partially negative epoxy and hydroxyl groups.[29] Note that the XPS characterization results indeed indicate that simple mixing of a GO and SnO_2 precursor solution not only leads to the reduction of GO to rGO, but also simultaneously results in the formation of SnO_2 nanoparticles. Based on our observation, the possible reaction mechanism[30] is proposed as follow: $Sn(CH_3COO)_2 + GO + H_2O \rightarrow SnO_2 + rGO + 2CH_3COOH$.

Owing to the effect of strong pseudocapacitive character of SnO_2 and the highly electro-conductive rGO support, hybrids are expected to be an excellent electrode material for supercapacitors. The performance of supercapacitor electrodes was analyzed using cyclic voltammetry (CV) and gavanostatic charge-discharge at room temperature. Typical three-electrode configuration was employed in 1 M H_2SO_4 electrolyte. Figure 4(a) and (b) show the CVs of the rGO and rGO-SnO_2 electrodes, scanned at various scan rates in a potential range of 0 to 1.0 V. The voltammograms of the rGO and rGO-SnO_2 exhibit a nearly rectangular shape, indicating a good capacitive behavior in the electrochemical supercapacitors.[31] The higher capacitive current and redox peaks are observed in the CV for the rGO-SnO_2, which are attributed to the efficient electric double layer capacitor performance of the carbon support and pseudocapacitive properties from redox reactions on tin oxide. The specific capacitances of electrode can be calculated according to the following equation:

$$C = (\int I\mathrm{d}V)/(v \cdot m \cdot V) \quad (2)$$

Where I is the response current (A), V is the potential (V), v is the potential scan rate (mV/s), and m is the mass of the electroactive materials in the electrodes (g). The specific capacitance values of rGO and rGO-SnO_2 electrodes at 50 mV/s are 241 and 389 F/g, respectively. Specific capacitance values of rGO and rGO-SnO_2 at various scan rates are compared in Figure 4(c). The rGO-SnO_2 electrode shows the enhanced capacitance performance for various scan rates. The rGO-SnO_2 composites exhibit high specific capacitance values from 477 to 362 F/g as the scan rate increases from 5 to 100 mV/s and maintain 75.9% of its specific capacitance at a high rate. The capacitance retention of 52.9% from 411 to 218 F/g at the rates from 5 to 100 mV/ s of the rGO electrode is shown in Figure 4(d). These results are due to the enhanced electrolyte accessibility, facilitated charge propagation along the hybrid electrode and the high electrochemical stability for the redox transition of electrodes at higher scan rates.

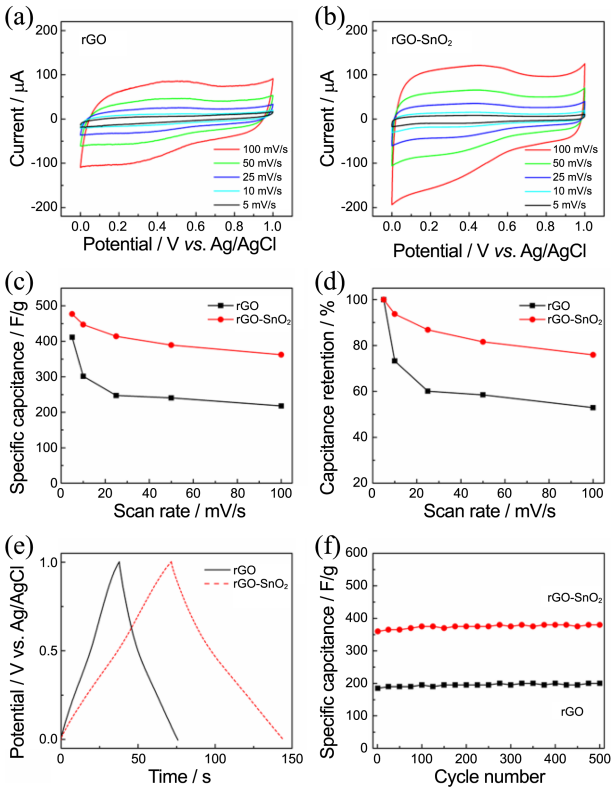

Figure 4. CV curves of annealed rGO (a) and rGO-SnO_2 nanocomposites (b) at various scan rates in 1 M H_2SO_4 electrolyte. (c) Specific capacitance at different scan rate of rGO and rGO-SnO_2 nanocomposites. (d) The capacitance retention ratio vs. scan rates of rGO and rGO-SnO_2. (e) Gavanostatic charge-discharge curves of rGO and rGO-SnO_2 in 1 M H_2SO_4 at 5 A/g. (f) Variation of the capacitance vs. cycle number of rGO and rGO-SnO_2.

Figure 4(e) shows the galvanostatic charge-discharge curves of rGO and rGO-SnO_2 electrodes at a current density of 5 A/g in a potential rage between 0 and 1.0 V. The galvanostatic curve of the hybrid is similar to that of rGO, which is linear and symmetrical, and shows no obvious iR drop, indicating low inter-resistance and instant I-V response of the hybrid.[32] Also, from the charge-discharge curves, the specific capacitance values were calculated according to the following equation:

$$C = I/(m(\Delta V/\Delta t)) \quad (3)$$

Where I is the constant current during discharge (A), and $\Delta V/\Delta t$ is the slope of the discharge curve (V/s). The specific capacitance of rGO and rGO-SnO_2 nanocomposites at 5 A/g was about 190 and 362 F/g, respectively. To further investigate the cyclability of rGO and the rGO-SnO_2 hybrid, the galvanostatic charge-discharge was performed for 500 cycles at 5 A/g (Figure 4(f)). During first 100 cycles the specific capacitance of rGO and rGO-SnO_2 increased about 2.6 and 2.4%, respectively. Such an increase in capacitance can be ascribed to an activation process, in which the active

materials become fully utilized in the electrochemical reaction.[33] After the entire activation, rGO and rGO-SnO_2 sustained the constant specific capacitance values, indicating the excellent cycle stability and high reversibility.

Conclusion

In summary, we have demonstrated the preparation of rGO-SnO_2 hybrid materials through a straightforward hybridization method. By simple mixing of GO and a SnO_2 precursor solution, a hybrid complex of GO-SnO_2 was achieved. In this hybrid process, the oxygen functional groups in GO played a key role in conversion of Sn^{2+} into SnO_2 nanoparticles. Furthermore, hybrids of rGO and SnO_2 produced *via* a facile solution-processing route showed enhanced electrochemical properties. Owing to the synergistic effects from carbon and metal oxide components, those hybrids demonstrate remarkable performance as supercapacitor electrodes. Therefore, this work has shown that GO is an excellent nanoplatform for hybrid nanocomposites for electrode applications. Our hybrid strategy not only provides a high throughput and scalable synthetic route, but also illustrates the effectiveness of oxygen functionalized graphene sheet (GO) for the synthesis of functional nanomaterials.

Acknowledgments. This work was financially supported by the startup grant from Hanyang University (HY-2012).

References

1. Brodie, B. C. *Philos. Philos. T. R. Soc.* **1859**, *149*, 249.
2. Hummers, W. S.; Offeman, R. E. *J. Am. Chem. Soc.* **1958**, *80*, 1339.
3. Li, D.; Kaner, R. B. *Science* **2008**, *320*, 1170.
4. Compton, C.; Nguyen, T. *Small* **2010**, *6*, 711.
5. Tung, V. C.; Allen, M. J.; Yang, Y.; Kaner, R. B. *Nat. Nanotechnol.* **2009**, *4*, 25.
6. Jeon, Y.; Shin, Y. R.; Sohn, J. H.; Choi, H. J.; Bae, S. Y.; Mahmood, J.; Jung, S. M.; Seo, J. M.; Kim, M. J.; Chang, D. W.; Dai, J. M.; Baek, J. B. P. *Nat. Acad. Sci. USA* **2012**, *109*, 5588.
7. Hernandez, Y.; Nicolosi, V.; Lotya, M.; Blighe, F. M.; Sun, Y.; De, S.; McGovern, I. C.; Holland, B.; Byrne, M.; Gun'ko, Y. K.; Boland, J. J.; Niraj, P.; Duesberg, G.; Krishnamurthy, S.; Goodhue, R.; Hutchison, J.; Scardaci, V.; Ferrari, A. C.; Coleman, T. N. *Nat. Nanotechnol.* **2008**, *3*, 563.
8. Stankovich, S.; Dikin, D. A.; Dommett, G. H. B.; Kohlhaas, K. M.; Zimney, E. J.; Stach, E. A.; Piner, R. D.; Nguyen, S. T.; Ruoff, R. S. *Nature* **2006**, *442*, 282.
9. Xu, Z.; Gao, C. *Nat. Commun.* **2011**, *2*, 571.
10. Kim, J. E.; Han, T. H.; Lee, S. H.; Kim, J. Y.; Ahn, C. W.; Yun, J. M.; Kim, S. O. *Angew. Chem. Int. Ed.* **2011**, *50*, 3043.
11. Han, T. H.; Huang, Y. K.; Tan, A. T. L.; Dravid, V. P.; Huang, J. *J. Am. Chem. Soc.* **2011**, *133*, 15264.
12. Han, T. H.; Lee, W. J.; Lee, D. H.; Kim, J. E.; Choi, E. Y.; Kim, S. O. *Adv. Mater.* **2010**, *22*, 2060.
13. Cheng, Q.; Tang, J.; Ma, J.; Zhang, H.; Shinya, N.; Qin, L. C. *Carbon* **2011**, *49*, 2917.
14. Lu, T.; Zhang, Y. P.; Li, H. B.; Pan, L. K.; Li, Y. L.; Sun, Z. *Electrochim. Acta* **2010**, *55*, 4170.
15. Wu, Z. S.; Wang, D. W.; Ren, W.; Zhao, J.; Zhou, G.; Li, F.; Cheng, H. M. *Adv. Funct. Mat.* **2010**, *20*, 3595.
16. Qiu, G. H.; Dharmarathna, S.; Zhang, Y. S.; Opembe, N.; Huang, H.; Suib, S. L. *J. Phys. Chem. C* **2012**, *116*, 468.
17. Zou, W. B.; Zhu, J. W.; Sun, Y. X.; Wang, X. *Mater. Chem. Phys.* **2011**, *125*, 617.
18. An, G. M.; Na, N.; Zhang, X. R.; Miao, Z. J.; Miao, S. D.; Ding, K. L.; Liu, Z. M. *Nanotechnology* **2007**, *18*, 435707.
19. Guo, Z. P.; Du, G. D.; Nuli, Y.; Hassan, M. F.; Liu, H. K. *J. Mater. Chem*. **2009**, *19*, 3253.
20. Wang, H. L.; Casalongue, H. S.; Liang, Y. Y.; Dai, H. J. *J. Am. Chem. Soc.* **2010**, *132*, 7472.
21. Ding, S. J.; Luan, D. Y.; Boey, F. Y. C.; Chen, J. S.; Lou, X. W. *Chem. Comm.* **2011**, *47*, 7155.
22. Li, F. H.; Song, J. F.; Yang, H. F.; Gan, S. Y.; Zhang, Q. X.; Han, D. X.; Ivaska, A.; Niu, L. *Nanotechnology* **2009**, *20*, 455602.
23. Han, T. H.; Oh, J. K.; Park, J. S.; Kwon, S. H.; Kim, S. W.; Kim, S. O. *J. Mater. Chem.* **2009**, *19*, 3512.
24. van Esch, J. H.; Feringa, B. L. *Angew. Chem. Int. Ed.* **2000**, *39*, 2263.
25. Weiss, R. G.; Terech, P. In *Molecular Gels*; Springer; 2006; Chapter 8.
26. Chen. S. Q.; Wang, Y. *J. Mater. Chem.* **2010**, *20*, 9735.
27. Wang, W. J.; Hao, Q. L.; Lei, W.; Xia, X. F.; Wang, X. *RSC Adv.* **2012**, *2*, 10268.
28. An, G. M.; Yu, P.; Xiao, M. J.; Liu, Z. M.; Miao, Z. J.; Ding, K. L.; Mao, L. Q. *Nanotechnology* **2008**, *19*, 275709.
29. Zhou, X.; Wan, L. J.; Guo, Y. G. *Adv. Mater.* **2013**, DOI 10. 1002/adma.201300071.
30. Song, H. J.; Zhang, L. C.; He, C. L.; Qu, Y.; Tian, Y. F.; Lv, Y. *J. Mater. Chem.* **2011**, *21*, 5972.
31. Stoller, M. D.; Park, S.; Zhu, Y. W.; An, J. H.; Ruoff, R. S. *Nano Lett.* **2008**, *8*, 3498.
32. Fan, Z. J.; Yan, J.; Wei, T.; Zhi, L. J.; Ning, G. Q.; Li, T. Y.; Wei, F. *Adv. Funct. Mater.* **2011**, *21*, 2366.
33. Dong, X. C.; Xu, H.; Wang, X. W.; Huang, Y. X.; Chan-Park, M. B.; Zhang, H.; Wang, L. H.; Huang, W.; Chen, P. *ACS Nano* **2012**, *6*, 3206.